RSC Advances

RSC Publishing

PAPER

View Article Online
View Journal | View Issue

Regular assembly of 9-fluorenone-2,7-dicarboxylate within layered double hydroxide and its solid-state photoluminescence: a combined experiment and computational study†

Cite this: *RSC Advances*, 2013, **3**, 4303

Dongpeng Yan,* Yibing Zhao, Min Wei, Ruizheng Liang, Jun Lu, David G. Evans and Xue Duan

The assembly of an organic dye molecule incorporated into inorganic host matrices has received considerable attention for developing new types of organic–inorganic hybrid photofunctional materials. In this work, we report 9-fluorenone-2,7-dicarboxylate (FDC) assembled into Mg-Al- and Zn-Al-layered double hydroxide (LDH) systems and their solid-state photophysical properties. The detailed structure and chemical compositions of the obtained composites were characterized by X-ray diffraction, elemental analysis, thermogravimetry and differential thermal analysis (TG-DTA), infrared spectra (IR) and ^{13}C nuclear magnetic resonance (NMR), which show that the positively-charged LDH layer can delocalize the electronic density of the anionic FDC to some extent. Moreover, FDC/LDH systems exhibit a blue-shift photoemission and enhanced fluorescence lifetime compared with those of the pristine FDC sample, and the FDC/LDH thin films exhibit well-defined polarized luminescence with the fluorescence anisotropy of 0.15–0.25. In addition, a periodic density functional theoretical (DFT) calculation was employed to calculate the geometric and electronic structures of the FDC/LDH systems. It was found that the FDC/LDH can be regarded as energy transfer systems from the interlayer organic chromophore to the inorganic host layer due to close energy levels between two components. Therefore, based on the combination of experimental and theoretical studies on the chromophore assembled LDH systems, this work not only gives a detailed investigation on the relationship between the layered host–guest structures and photoluminescence properties, but also provides a new insight into the energy-transfer performance of guest dye molecules confined between the 2D inorganic host matrix.

Received 26th November 2012,
Accepted 18th January 2013

DOI: 10.1039/c3ra23064c

www.rsc.org/advances

1 Introduction

The assembly of an organic dye molecule incorporated into inorganic host matrices[1] has received considerable attention owing to the advantages as follows: firstly, the orderly distribution and arrangement of dye molecules within the regular framework are favorable for the improvement of luminescent efficience of the organic–inorganic hybrid materials, which is a prerequisite for constructing a new generation of solid-state dye laser and dye-based molecular optical devices;[2] secondly, the solid matrices can offer a higher mechanical, thermal and chemical stability for the dye molecules;[3] and last but not least, the immobilization of a dye in the hybrid materials based on host–guest interactions also reduces the environmental pollution and/or operational risk, which is beneficial to their practical application as solid-state optoelectronic devices.[4] In this sense, layered double hydroxides (LDHs) are one typical two-dimensional (2D) host matrix, which can be described by the general formula $[M^{II}_{1-x}M^{III}_{x}(OH)_2][A^{n-}_{x/n}\cdot mH_2O]$, where M^{II} and M^{III} are divalent and trivalent metals, respectively, and A^{n-} is an anion. The positively-charged host layers are electrically balanced by anions in the interlayer space,[5] and the functional anions can be assembled within LDHs for constructing new types of organic–inorganic hybrid materials.[6] Unlike most cationic clay materials, an important feature of LDHs is that the layered charge density and the chemical composition can be tuned over a wide range during synthesis, which facilities fine control of the properties of LDH-based materials.[5e] Recently, LDHs have been paid much interest in the fields of catalysis,[7] separation,[8] photochemical cells[9] and drug delivery.[10] Moreover, LDH-based luminescence (such as chemilu-

State Key Laboratory of Chemical Resource Engineering, Beijing University of Chemical Technology, Beijing 100029, P. R. China. E-mail: yandp@mail.buct.edu.cn; yandongpeng001@163.com; Fax: +86-10-64425385; Tel: +86-1064412131

† Electronic supplementary information (ESI) available: Total and partial electronic density of states (TDOS and PDOS) profiles for different atoms in pristine FDC (Fig. S1), FDC/Mg_2Al-LDH (Fig. S2), FDC/Zn_2Al-LDH (Fig. S3). See DOI: 10.1039/c3ra23064c

minescence and photoluminescence) systems have been extensively investigated.[11,12] For example, Lu and co-workers[11] have developed several anionic surfactant-intercalated LDH systems, which significantly enhance the chemiluminescence intensity compared with the pure anionic surfactants due to the disappearance of electrostatic repulsion between surfactants and chemiluminescence reactants. In contrast to chemiluminescence, the photoluminescence (or fluorescence) usually involves a photoexcitation/emission process without the occurrence of an oxidation/reduction chemical reaction. A series of fluorescence dye molecules intercalated in LDH materials exhibited several new photophysical properties compared with those of the pristine dye systems. For example, Lang *et al.*[12k,l] have reported that anionic porphyrin molecules intercalated in LDH can produce $O_2(^1\Delta_g)$ with longer lifetimes. Costantino *et al.*[12a] have observed that the emission spectrum of methyl orange-intercalated LDH exhibited a red-shift compared with that of a dilute solution. Furthermore, it was demonstrated that the luminescent properties and the molecular alignment of dyes can be tuned to some extent upon assembly into the LDH layer.[12j] However, the reported asymmetric dye anions (such as rhodamine B[4] and fluorescein[12b]) usually result in a relative random transition dipole of the molecules within the 2D interlayer, which is unfavorable for the construction of highly-orientational polarized materials. For example, a broad distribution of the molecular orientation of the dye molecules can still be observed;[12h] therefore, the design and synthesis of new luminescent dye/LDH systems with a well-organized and highly-ordered structure continue to be a stimulating challenge.

Fluorenone and its derivatives are important chromophore molecules with intriguing photophysical performance,[13] which have been studied, developed and applied as a new type of solid-state fluorescent materials. To the best of our knowledge, however, research on the incorporation of fluorenone-based dye into the gallery of LDHs has never been reported. In this work, organic anion, 9-fluorenone-2,7-dicarboxylate (FDC, shown in Scheme 1), intercalated Mg_2Al-LDH and Zn_2Al-LDH systems have been synthesized. The rational selection of a M^{II}/M^{III} ratio of 2 is due to the highly-ordered structure within the LDH layer.[14] In addition, compared with other non-planar and unsymmetrical dye molecules (*e.g.*, rhodamine), FDC is a centrally symmetrical anion with rigid planarity and two carboxylates at ends of the molecule, which allows FDC anions to adopt a vertical orientation relative to the LDH layer with the aid of two carboxylates anchored to the LDH layer. This property is undoubtedly favorable to produce a highly ordered orientation of transition dipole moment for polarized photoemission. Moreover, the detailed structure, thermal stability and photophysical properties of FDC/LDH systems were studied by NMR, FT-IR, thermogravimetric and differential thermal analysis (TG-DTA) and fluorescence spectroscopy. It was observed that the FDC/LDHs feature a blue-shift photoemission and enhanced fluorescence lifetime compared with the pure FDC molecule, and FDC/LDH thin films exhibit well-defined polarized photoemission anisotropy. In addition, a periodic density functional theoretical (DFT) calculation was performed to analyze the geometric and electronic structures of both the pure FDC and FDC/LDH systems. The computational results showed that LDH-based organic–inorganic hybrid materials can serve as energy transfer systems from the interlayer organic chromophore to the inorganic host layer. Therefore, this work provides a feasible route for combining an experimental methodology and theoretical study for designing and understanding the orderly structure and the regular alignment of photofunctional species assembled in the LDH matrix. It is also expected that the FDC/LDH hybrid systems can be potentially applied in the field of polarized emission and energy transfer materials.

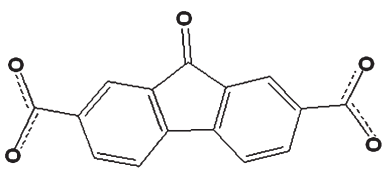

Scheme 1 The molecular structure of 9-fluorenone-2,7-dicarboxylate.

2 Experimental

2.1 Reagents and materials

9-Fluorenone-2,7-dicarboxylic acid (H_2FDC, 90%) was purchased from J&K Chemical Co. Ltd. NaOH (AR), $Al(NO_3)_3\cdot 9H_2O$ (AR), $Zn(NO_3)_2\cdot 6H_2O$ (AR) and $Mg(NO_3)_2\cdot 6H_2O$ (AR) were purchased from the Beijing Chemical Co. Limited, and used without further purification. Carbonate-free deionized water was used throughout the experimental processes.

2.2 Synthesis of FDC/Mg_2Al-LDH and FDC/Zn_2Al-LDH.

The sodium salt of H_2FDC (Na_2FDC) was prepared by neutralizing H_2FDC with NaOH following Furman's previous work.[13b] Then, FDC anion-intercalated Mg_2Al-LDH and Zn_2Al-LDH were prepared by a coprecipitation method. The matched molar ratios of Mg^{2+} (Zn^{2+})/Al^{3+}/OH^-/FDC were 2.0 : 1.0 : 6.0 : 0.5. Typically, a 100 mL solution containing 5 mmol $Mg(NO_3)_2\cdot 6H_2O$ (or $Zn(NO_3)_2\cdot 6H_2O$) and 2.5 mmol $Al(NO_3)_3\cdot 9H_2O$ was slowly added dropwise to a 100 mL solution containing 15 mmol NaOH and 1.25 mmol Na_2FDC with vigorous agitation under a nitrogen flow. The pH value at the end of addition was adjusted to 8.0 by further addition of 2.4 mol L^{-1} NaOH solution. The reaction mixture was subsequently heated at 70 °C for 24 h, washed thoroughly with deionized water and dried at 70 °C for 16 h under vacuum condition. Based on the results of elemental analysis (Mg 14.31%, Al 7.77%, C 25.94%, and H 4.01% for FDC/Mg_2Al-LDH; Zn 31.62%, Al 5.99%, C 19.98%, and H 3.47% for FDC/Zn_2Al-LDH), the chemical compositions can be determined as: $Mg_{2.023}Al_{0.977}(OH)_6(C_{15}H_6O_5)_{0.489}\cdot 2.337H_2O$ and $Zn_{2.060}Al_{0.940}(OH)_6(C_{15}H_6O_5)_{0.470}\cdot 2.587H_2O$ for FDC/Mg_2Al-LDH and FDC/Zn_2Al-LDH, respectively. The water content was determined by TG-DTA analysis with the assumption that

the interlayer water molecules are totally evaporated before 190 °C. The LDH films were prepared by the solvent evaporation method. Typically, an ethanol suspension of FDC/LDH (1 mg mL^{-1}) was thoroughly dispersed under ultrasonication and then placed on a quartz substrate.

2.3 Characterization

The XRD measurements were performed on a Rigaku XRD-6000 diffractometer, using Cu-Kα radiation (λ = 0.15418 nm) at 40 kV and 30 mA, with a scanning rate of 10° min^{-1}, and the 2θ angle ranging from 3 to 70°. Fourier-transfer infrared (FT-IR) spectra were recorded on a Bruker Vector 22 using the KBr disk method in the range from 4000 to 400 cm^{-1}, with a resolution of 2 cm^{-1} and an accumulation of 32 scans. Solid-state cross-polarization/magic angle spinning (CP/MAS) ^{13}C nuclear magnetic resonance (NMR) spectra were recorded using a Bruker BioSpin AV 300 MHz at 20 °C with a 4 mm rotor spinning at 5 kHz under a static magnetic field of 9.4 T. ^{13}C spectra were obtained at the frequency of 75.48 MHz with a 5 s relaxation delay and a spectral bandwidth of 350 ppm. TG-DTA was measured on a PCT-1A thermal analysis system under ambient atmosphere with a heating rate of 10 °C min^{-1}. Elemental analysis (Mg, Al, Zn) was performed by atomic emission spectroscopy with a Shimadzu ICPS-7500 instrument. C, H, N contents were determined using a Perkin Elmer Elementarvario elemental analysis instrument. The fluorescence spectra were performed on a Hitachi F-7000 FL spectrophotometer with a slit width of 3 nm, excitation at 360 nm and a PMT voltage of 400 V. Fluorescent lifetime measurements were recorded with an Edinburgh Instruments FL 900 fluorimeter. The percentage contribution of each lifetime component to the total decay was calculated with the Edinburgh F900 instruments software. Steady-state polarized photoluminescence measurements were recorded with an Edinburgh Instruments' FLS 920 fluorimeter.

2.4 Structure model and computational method

An ideal LDH layer model with tetragonal superlattice and $R\bar{3}m$ space group was built based on the previous work.[12g,h] The lattice parameters of the two-dimensional layer are $a = b$ = 3.05 Å, in accordance with other literatures.[15] Each octahedral layer contains 8 Mg, 4 Al atoms and 24 OH groups, and a supercell was constructed with the lattice parameters a = 10.57 Å, b = 9.15 Å and the initial interlayer spacing c = 17.8 Å (experimental result), $\alpha = \beta = 90°$, $\gamma = 120°$ (equivalent to 4 × 3 × 1 supercell). The supercell was treated as P1 symmetry, and a three-dimensional periodic boundary condition was applied.[16] Then, two FDC ($C_{15}H_6O_5$) anions with two negative charges each, were introduced into the simulated supercell. As a result, the formula of the simulated structure can be expressed as: $Mg_8Al_4(OH)_{24}(C_{15}H_6O_5)_2$ or $Zn_8Al_4(OH)_{24}(C_{15}H_6O_5)_2$. All calculations were performed with the periodic density functional theory (DFT) method using the Dmol3[17a,b] module in the Material Studio software package.[17c] The initial configuration was first fully optimized with fixed positions for the atoms in the layer by the classical molecular mechanics method employing a cff91 force field,[17d,e,f] and then further optimization was implemented by the Perdew-Wang (PW91)[17g] generalized gradient approximation (GGA) method with the double numerical basis sets plus polarization function (DNP). The core electrons for metals were treated by effective core potentials (ECP). The SCF-converged criterion was within 1.0 × 10^{-5} hartree $atom^{-1}$ and converged criterion of structure optimization was 1.0 × 10^{-3} hartree $bohr^{-1}$. The Brillouin zone is sampled by 1 × 1 × 1 k-points, and test calculations reveal that the increase of k-points does not affect the results.

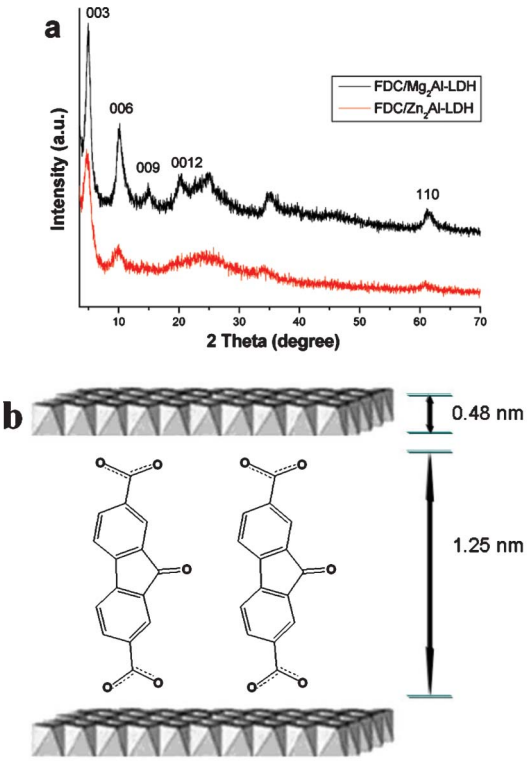

Fig. 1 (a) XRD patterns of FDC/Mg_2Al-LDH and FDC/Zn_2Al-LDH. (b) The structural model of FDC/Mg_2Al-LDH.

3 Results and discussion

3.1 Structural characterization of FDC-intercalated Mg-Al-LDH and Zn-Al-LDH

The powder XRD patterns of FDC/Mg_2Al-LDH and FDC/Zn_2Al-LDH are shown in Fig. 1a. In this case, all the reflections can be indexed to a rhombohedral lattice with $R\bar{3}m$ symmetry, which is commonly used for the description of the 3R-type LDH structure. Taking FDC/Mg_2Al-LDH as the example, the main characteristic reflections appear at 4.92° (003), 10.08° (006), 14.86° (009), 20.21° (0012) and 61.12° (110), respectively. Values of d_{003} (1.791 nm), d_{006} (0.875 nm) and d_{009} (0.954 nm) present a good multiple relationship between the basal, second and third-order reflections. The lattice parameter c can be calculated from averaging the positions of the three harmonics: $c = 1/3\ (d_{003} + 2d_{006} + 3d_{009})$ = 1.775 nm, which is consistent with the vertical arrangement fashion of the FCB/LDH supramolecular structure with the thickness of about

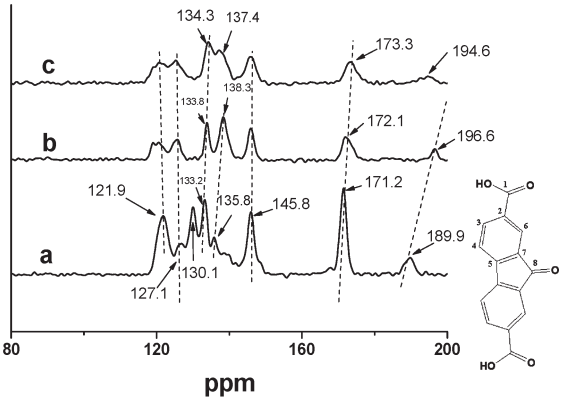

Fig. 2 ^{13}C MAS NMR spectra for (a) the pristine FDC, (b) FDC/Mg_2Al-LDH and (c) FDC/Zn_2Al-LDH.

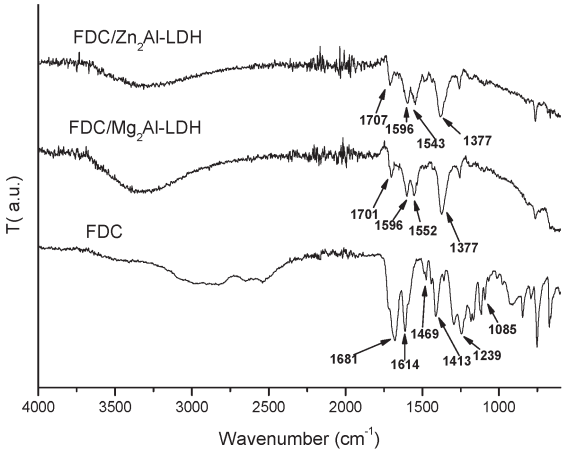

Fig. 3 FT-IR spectra for (a) the pristine FDC, (b) FDC/Mg_2Al-LDH and (c) FDC/Zn_2Al-LDH.

0.48 nm for an LDH layer and 1.25 nm for the length of the FDC anion in the long-axis direction as shown in Fig. 1b. For the sample of the FDC/Zn_2Al-LDH, the crystallinity was relatively poor compared with that of FDC/Mg_2Al-LDH. The basal and second reflections were observed at 4.90° (1.798 nm) and 9.96° (0.886 nm), and the basal spacing is 1.785 nm. The lattice parameter a, corresponding to the shortest distance of adjacent metal atoms with identical chemical environment in the LDH layer, can be calculated by: $a = 2d_{110}$. The value of a for the two samples is 3.03 Å, in accordance with other reported LDH system (3.04 or 3.05 Å).[18]

Solid-state NMR is a powerful method for characterizing organic–inorganic solid materials and understanding the host–guest interactions and molecular packing.[19] Fig. 2 shows the experimental ^{13}C MAS NMR spectra of the pristine FDC and FDC/LDH composites. For the pristine FDC sample, eight resonance peaks appear at 121.9, 127.1, 130.1, 133.2, 135.8, 145.8, 171.2 and 189.9 ppm, corresponding to the C_4, C_2, C_6, C_3, C_7, C_5, C_1 and C_8 atoms respectively as shown in the inset of Fig. 2. Upon intercalation into the Mg_2Al-LDH layer, no chemical shift occurs for the sp^2 C_4, C_2 and C_5 atoms in the FDC anion, while those of C_3, C_7 and C_1 atoms are shifted downfield at 133.8, 138.3 and 172.1 ppm. In particular, the peak of the C_8 atom moved by 6.7 ppm, and similar behavior can also be observed in the FDC/Zn_2Al-LDH system. The significant difference in the NMR spectral features between the FDC and FDC/LDH can be attributed to host–guest electrostatic interaction, suggesting that the positively-charged LDH layer can polarize and delocalize the electronic density of the anionic FDC to some extent.

Fig. 3 shows the FT-IR spectra of pristine FDC and the FDC/LDH samples. The IR bands are assigned based on the literatures.[20] For the pristine FDC, the bands at 1681 and 1614 cm^{-1} are attributed to the vibrations of C=O in $-COO^-$ group, and the band at 1413 cm^{-1} due to the symmetric stretching vibration of C–O in the $-COO^-$ can also be observed. The band at 1469 cm^{-1} corresponds to the skeleton vibration of the phenyl ring. The in-plane bending vibrations of =C–H in the phenyl ring appear at 1238 and 1085 cm^{-1}, respectively. When the FDC anion was intercalated into Mg_2Al-LDH layer, only one band was resolved as the vibration of C=O, with a blue shift from 1681 to 1701 cm^{-1} (Δ = 20 cm^{-1}), indicating a strong electrostatic interaction between the carboxylate group and the Mg-Al-hydroxyl layers. The bands at 1596 and 1552 cm^{-1} are assigned to the stretching vibration of the phenyl ring. The FT-IR spectrum of the FDC/Zn_2Al-LDH sample exhibits a similar spectral feature as that of the FDC/Mg_2Al-LDH, indicating that FDC anions have a similar interlayer environment within both the Mg_2Al-LDH and Zn_2Al-LDH layers. The vibration of C=O of $-COO^-$ is located at 1707 (Δ = 6 cm^{-1}), compared with that of the FDC/Mg_2Al-LDH sample, illustrating that the interaction between the carboxylate group and LDH layers can be influenced by the elemental compositions of the LDH layer. The lattice vibration of the inorganic LDH layers can be observed in the region from 400 to 800 cm^{-1}. Moreover, the vibration bands of FDC become relatively weak and broad upon intercalation, indicating that the rigid LDH host can suppress the vibration of the FDC backbone based on electrostatic and/or van der Waals interactions.

3.2 Thermal decomposition of FDC and FDC/LDH

The thermolysis process of both the FDC and FDC/LDH was studied by analyzing their TG-DTA curves. Fig. 4a shows the typical TG-DTA profiles for the FDC sample. It was found that only 5.3% of thermolysis can be observed until the temperature increases to *ca.* 290 °C. The sharp weight loss of 91.5% in the region 290–650 °C with a broad exothermic range (exothermic peak: 476 °C) in the DTA curve is assigned to the decomposition and combustion of FDC. For the sample of FDC/Mg_2Al-LDH (Fig. 4b), the thermal decomposition behavior can be recognized by three weight loss steps. The first one is in the range from room temperature to 190 °C accompanying the weight loss of 12.4%, which is due to the removal of surface adsorbed and interlayer water molecules. The second one, with a gradual weight loss of 8.7% in the temperature range 190–390 °C, can be attributed to the decomposition and dehydroxylation of the brucite-like layers. The third one, in the range 390–650 °C, corresponds to the decomposition and/or combustion of FDC and collapse of the layer, which features a

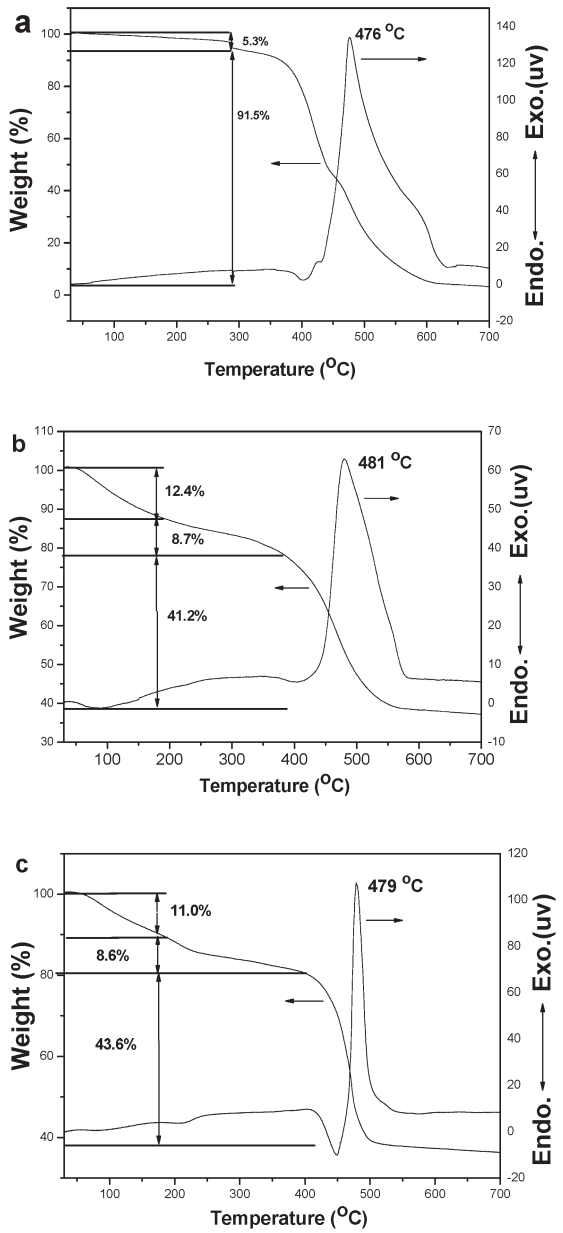

Fig. 4 TG and DTA curves for (a) pristine FDC, (b) FDC/Mg_2Al-LDH, and (c) FDC/Zn_2Al-LDH.

strong exothermic peak at *ca.* 481 °C in the DTA curve. TG-DTA curves of FDC/Zn_2Al-LDH were shown in Fig. 4c, from which it can be observed that three weight losses of 11.0, 8.6 and 43.6% occur in the temperature ranges 30–190, 190–400 and 400–650 °C, respectively. In addition, the strong and sharp exothermic peak corresponding to the combustion of interlayer FDC appears at 479 °C; therefore, it can be concluded that there is no obvious enhancement of the thermal stability of the FDC molecule after intercalation. Since most reported dye/LDH systems[4,12g,h,j] show that the combustion temperature of guest anions increases effectively within the LDH layer, this somewhat unexpected result for the FDC/LDH system can be attributed to FDC being a large π-conjugated system with

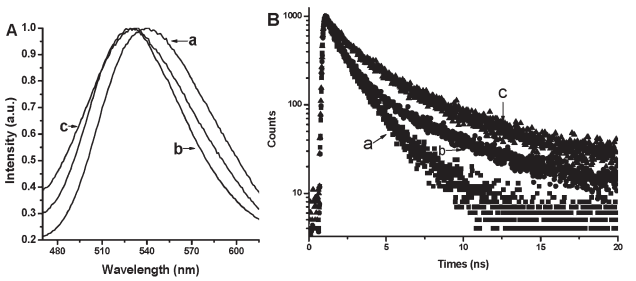

Fig. 5 (A) Fluorescence emission spectra and (B) fluorescence decay curves for pristine FDC (a), FDC/Mg_2Al-LDH (b) and FDC/Zn_2Al-LDH (c).

strong intermolecular interactions. In our opinion, for the pristine FDC, the strong hydrogen bonding and π–π interactions between the planar molecule predominate throughout the organic solid; while in the case of FDC/LDH, the host–guest interactions (mainly electrostatic interactions and hydrogen bonding between LDH layers and FDC anions) regulate the parallel arrangement of interlayer FDC, and the favorable guest–guest interactions (mainly π–π interactions) are relatively suppressed.

3.3 Photophysical properties of FDC/LDH

Fig. 5A shows the fluorescence emission spectra of the pristine FDC and FDC/LDH sample. For the pristine FDC solid sample, the symmetrical emission peak can be observed at 540 nm (Fig. 5A(a)) with the FWHM of 101 nm. Moreover, the emission peaks of FDC/Mg_2Al-LDH and FDC/Zn_2Al-LDH appeared at 529 and 531 nm with the FWHM of *ca.* 88 and 111 nm, respectively (Fig. 5A(b and c)). Generally, two types of aggregates of dye dimer can form depending on the angle between the transition dipole and the lineation of centers vector of the two dye molecules. They are named as *H*-type (face-to-face arrangement) and *J*-type (tail-to-tail arrangement) dimers, responsible for the blue and red shifts in the emission property of dye molecules, respectively. Therefore, herein, the blue-shift of the spectra for the FDC/LDH samples may be attributed to the formation of the *H* aggregate with π–π or dipole–dipole interaction in the gallery of the LDH layer. This phenomenon is also consistent with the vertical orientational arrangement of the FDC with respect to the LDH layer as deducted from the XRD result. To better understand the excited-state information of fluorescence for both the organic and organic–inorganic hybrid solids, the fluorescence lifetimes were determined and the corresponding fluorescence decay curves are shown in Fig. 5B. The fluorescence lifetime of pure FDC (Fig. 5B(a)) is 1.38 ns, whereas for FDC/Mg_2Al-LDH (Fig. 5B(b)) and FDC/Zn_2Al-LDH (Fig. 5B(c)) with low-wavelength emission, the values are 1.45 and 2.63 ns, suggesting the intercalation of the guest dye molecules within the layer matrix can stabilize the excited-state of the chromophores effectively. This fact can be attributed to the fact that the rigid and confined space imposed by LDH layers can suppress the thermal vibration and rotation of guest FDC anions relating to the non-radiative relaxation process (such as excitonic coupling and excimer formation) in their exciting states.

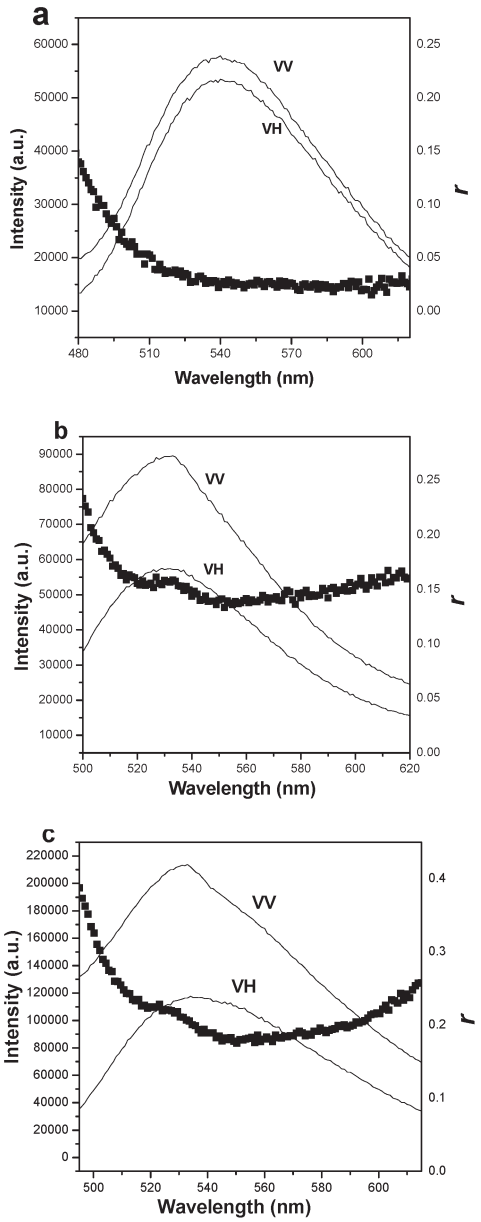

Fig. 6 Photoemission profiles in the VV, VH polarizations and anisotropic value (r) measured at room temperature (293 K) for: (a) the pristine FDC sample, (b) the FDC/Mg_2Al-LDH thin film, and (c) the FDC/Zn_2Al-LDH thin film.

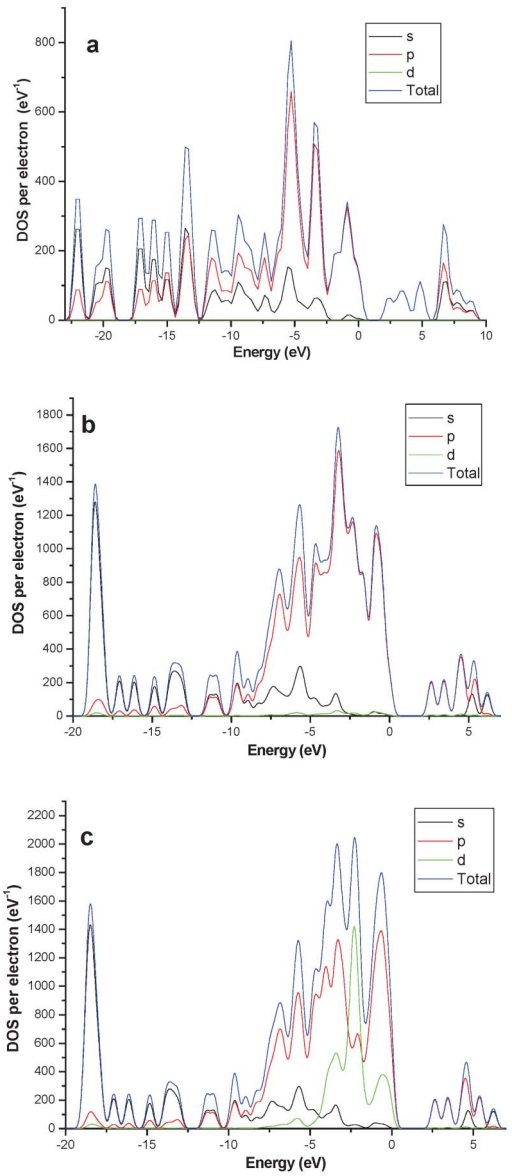

Fig. 7 Total and partial electronic density of state (TDOS and PDOS) for (a) pristine FDC, (b) FDC/Mg_2Al-LDH, and (c) FDC/Zn_2Al-LDH systems. Fermi energy level (E_F) was set as zero.

To further probe the preferred orientation and polarized luminescence properties, FDC/LDH films were fabricated by the solvent evaporation method. The anisotropic value r was determined;[21] r can be expressed as the formula: $r = \frac{I_{VV} - GI_{VH}}{I_{VV} + 2GI_{VH}}$, where $G = \frac{I_{HV}}{I_{HH}}$; I_{VH} stands for the photoluminescence intensity obtained with vertical polarized light excitation and horizontal polarization detection, and I_{VV}, I_{HH} and I_{HV} are defined in a similar way. For the pristine FDC sample (Fig. 6a), the r value was *ca.* 0.02–0.03 in the range 510–600 nm, indicating its isotropy. However, the r values are largely improved in the range 0.15–0.25 for the FDC/Mg_2Al-LDH (Fig. 6b) and FDC/Zn_2Al-LDH (Fig. 6c) samples, with an enhancement of at least 5 times upon intercalation. This indicates the highly-ordered arrangement of the FDC anions in the LDH gallery and confirms that the dye/LDH thin film exhibits a well-oriented and uniformly-ordered structure, consistent with the XRD observation.

3.4 The calculation of the electronic structure

To further study the geometric and electronic structures of the FDC/LDH systems, a periodic density functional theoretical (DFT) calculation was employed for the idealized model of pristine FDC and FDC/LDH structures. Total electronic densities of states (TDOS) and partial electronic densities of states (PDOS) analyses on different atoms (Fig. 7a and Fig. S1 in electronic supplementary information (ESI†)) reveal that the HOMO–1 was mainly distributed on the 2p orbitals of C and O

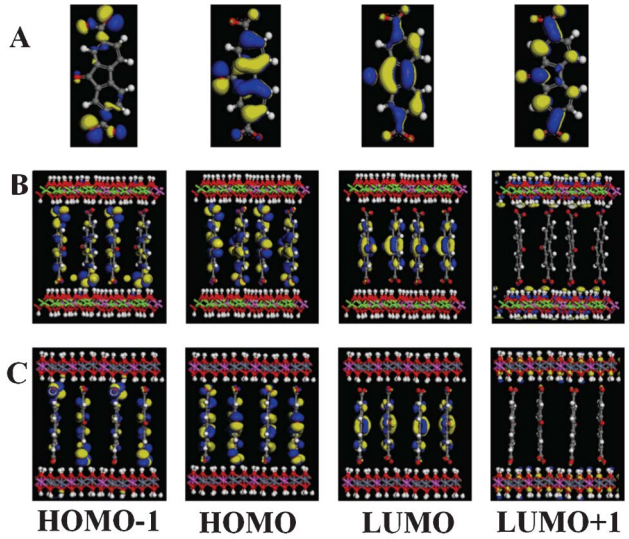

Fig. 8 Frontier orbital profiles (HOMO-1, HOMO, LUMO, LUMO+1) for (a) the pristine FDC, (b) FDC/Mg_2Al-LDH, and (c) FDC/Zn_2Al-LDH.

atoms in the carboxylate group of FDC, whereas the HOMO, LUMO and LUMO+1 are mainly dominated by the 2p(π) and 2p(π^*) C atomic orbitals in the main fluorenone skeleton. This can be further visualized by observing the frontier orbital profiles of FDC as shown in Fig. 8A. For the FDC/Mg_2Al-LDH system (Fig. 7b and Fig. S2 in ESI†), the optimized geometry (Fig. 8B) demonstrates that the FDC exhibits a vertical arrangement relative to the LDH layer and the anions are parallel with each other in the LDH gallery, in agreement with the XRD and fluorescence spectra results. Moreover, the HOMO-1, HOMO and LUMO are mainly dominated by the 2p(π) and 2p(π^*) atomic orbitals of C and 2p atomic orbitals of O atoms in the FDC molecules, respectively, while the LUMO+1 are mainly populated on the O and H atoms in the LDH layer (Fig. 7b and Fig. 8B). The energy band gap between the top of the valance band (TVB) and the bottom of the conducting band (BCB) is *ca.* 2.3 eV. Around the Fermi level, the TDOS are mainly consisted of the 2p electrons of C atoms in FDC. Similar behaviors can also be observed in the FDC/Zn_2Al-LDH systems (Fig. 7c, Fig. 8C, and Fig. S3 in ESI†), in which the 3d orbitals from the Zn atom also contribute to a part of TDOS near the Fermi level. Therefore, it can be concluded that the FDC/LDH systems exhibit an energy transfer behavior from the interlayer chromophores to the LDH layer owing to the close energy levels between the π-conjugated FDC and the LDH layer. Moreover, although confined effects (such as multiple quantum well)[22] based on host–guest interaction have already been investigated for other dye/LDH system, there are very few observations on such energy transfer systems based on host–guest intercalation structures. Compared with the typical dye-sensitized inorganic semiconductor systems,[23] such layered organic–inorganic hybrid systems may feature highly structural order and enhanced excited-state stability. Additionally, the interlayer content of the dye molecule, the layered element and charge density can also be fine-tuned.

4 Conclusions

In summary, the detained structural features and photoluminescence properties of FDC anion-intercalated Mg-Al-LDH and Zn-Al-LDH samples have been investigated. The FDC/LDH systems exhibit a blue-shift photoemission and enhanced fluorescence lifetime compared with the pristine FDC samples, indicating that the assembly of organic chromophores within the LDH layer can reduce the non-radiative relaxation process in the excited states of interlayer dye molecules. The polarized photoemission measurements show that the macroscopic anisotropy of the FDC/LDH films is improved significantly compared with the pristine FDC sample, suggesting that the uniform and ordered assembly of FDC can be achieved in the LDH gallery. DFT calculations demonstrated that the FDC/LDH has a low band gap. Moreover, the energy transfer process occurs from the interlayer dye molecules to the LDH layer, indicating the dye/LDH systems may have potential applications in the field of energy conversion and/or light-harvesting materials. Furthermore, it can be expected that by rationally designing and tuning the component, diversity and even the energy level of the dye molecule in the gallery of LDH with different alignments and assembly architectures, other similar ordered dye/LDH systems can be constructed, in which the improvement of light-emitting stability and energy transfer from organic to inorganic component can be achieved. Moreover, the electronic structures of the LDH can be tuned by controlling the LDH layers with different element compositions. This may open new ways to design and construct layered organic–inorganic hybrid structures for the fabrication of dye-based energy transfer systems into opto-electrical fields.

Acknowledgements

This work was supported by the National Natural Science Foundation of China, the 973 Program (Grant No. 2011CBA00504), 111 Project (Grant No. B07004), and Program for Changjiang Scholars and Innovative Research Team in University (PCSIRT: IRT1205).

References

1 (*a*) G. Ihlein, F. Schüth, O. Krauû, U. Vietze and F. Laeri, *Adv. Mater.*, 1998, **10**, 1117; (*b*) B. J. Scott, G. Wirnsberger, M. D. McGehee, B. F. Chmelka and G. D. Stucky, *Adv. Mater.*, 2001, **13**, 1231; (*c*) G. Calzaferri, S. Huber, H. Maas and C. Minkowski, *Angew. Chem., Int. Ed.*, 2003, **42**, 3732; (*d*) M. Busby, A. Devaux, C. Blum, V. Subramaniam, G. Calzaferri and L. De Cola, *J. Phys. Chem. C*, 2011, **115**, 5974; (*e*) C. A. Strassert, C.-H. Chien, M. D. G. Lopez, D. Kourkoulos, D. Hertel, K. Meerholz and L. De Cola, *Angew. Chem., Int. Ed.*, 2011, **50**, 946.

2 (*a*) C. M. Carbonaro, A. Anedda, S. Grandi and A. Magistris, *J. Phys. Chem. B*, 2006, **110**, 12932; (*b*) I. García-Moreno, A. Costela, A. Cuesta, O. García, D. del Agua and R. Sastre, *J. Phys. Chem. B*, 2005, **109**, 21618; (*c*) D. P. Yan, G. O. Lloyd,

A. Delori, W. Jones and X. Duan, *ChemPlusChem*, 2012, **77**, 1112.
3 M. Ogawa and K. Kuroda, *Chem. Rev.*, 1995, **95**, 399.
4 D. P. Yan, J. Lu, M. Wei, D. G. Evans and X. Duan, *J. Phys. Chem. B*, 2009, **113**, 1381.
5 (*a*) S. P. Newman and W. Jones, *New J. Chem.*, 1998, **22**, 105; (*b*) *Layered Double Hydroxides: Present and Future*, ed. V. Rives, Nova Science Publishers, New York, 2001; (*c*) B. M. Choudary, B. Bharathi, Ch. Venkat Reddy, M. L. Kantam and K. V. Raghavan, *Chem. Commun.*, 2001, 1734; (*d*) B. M. Choudary, M. L. Kantam, A. Rahman, Ch. Venkat Reddy and K. K. Rao, *Angew. Chem., Int. Ed.*, 2001, **40**, 763; (*e*) D. P. Yan, J. Lu, J. Ma, M. Wei, D. G. Evans and X. Duan, *Chem. Commun.*, 2010, **46**, 5912.
6 (*a*) A. I. Khan and D. O'Hare, *J. Mater. Chem.*, 2002, **12**, 3191; (*b*) F. Leroux and C. Taviot-Guého, *J. Mater. Chem.*, 2005, **15**, 3628; (*c*) F. Li and X. Duan, *Struct. Bonding*, 2006, **119**, 193; (*d*) D. G. Evans and X. Duan, *Chem. Commun.*, 2006, 485; (*e*) A. I. Khan, A. Ragavan, B. Fong, C. Markland, M. O' Brien, T. G. Dunbar, G. R. Williams and D. O'Hare, *Ind. Eng. Chem. Res.*, 2009, **48**, 10196; (*f*) X. Guo, F. Zhang, D. G. Evans and X. Duan, *Chem. Commun.*, 2010, **46**, 5197; (*g*) S. Ma, L. Du, J. Wang, N. Chu, Y. Sun, G. Sun, X. Yang and K. Ooi, *Dalton Trans.*, 2011, **40**, 9835; (*h*) Q. Wang, S. V. Y. Tang, E. Lester and D. O'Hare, *Nanoscale*, 2013, **5**, 114.
7 (*a*) B. F. Sels, D. E. De Vos and P. A. Jacobs, *Angew. Chem., Int. Ed.*, 2005, **44**, 310; (*b*) F. Winter, A. J. Van Dillen and K. P. De Jong, *Chem. Commun.*, 2005, 3977; (*c*) X. D. Lei, F. Z. Zhang, L. Yang, X. X. Guo, Y. Y. Tian, S. S. Fu, F. Li, D. G. Evans and X. Duan, *AIChE J.*, 2007, **53**, 932; (*d*) Y. Zhao, S. Zhang, B. Li, H. Yan, S. He, L. Tian, W. Shi, J. Ma, M. Wei, D. G. Evans and X. Duan, *Chem.–Eur. J.*, 2011, **17**, 13175.
8 (*a*) G. Centi and S. Perathoner, *Catal. Today*, 2003, **79–80**, 3; (*b*) M. Shao, F. Ning, J. Zhao, M. Wei, D. G. Evans and X. Duan, *J. Am. Chem. Soc.*, 2012, **134**, 1071.
9 (*a*) J. H. Lee, J. Chang, J.-H. Cha, D.-Y. Jung, . S. S. Kim and J. M. Kim, *Chem.–Eur. J.*, 2010, **16**, 8296; (*b*) T. Kameyama, K. Okazaki, K. Takagia and T. Torimoto, *Phys. Chem. Chem. Phys.*, 2009, **11**, 5369.
10 J.-H. Choy, S.-Y. Kwak, Y.-J. Jeoing and J.-S. Park, *Angew. Chem., Int. Ed.*, 2000, **39**, 4041.
11 (*a*) M. C. Zhang, D. M. Han, C. Lu and J.-M. Lin, *J. Phys. Chem. C*, 2012, **116**, 6371; (*b*) L. Zhang, Z. Zhang, C. Lu and J.-M. Lin, *J. Phys. Chem. C*, 2012, **116**, 14711; (*c*) Z. H. Wang, F. Liu and C. Lu, *Chem. Commun.*, 2011, **47**, 5479.
12 (*a*) U. Costantino, N. Coletti, M. Nocchetti, G. G. Aloisi and F. Elisei, *Langmuir*, 1999, **15**, 4454; (*b*) U. Costantino, N. Coletti, M. Nocchetti, G. G. Aloisi, F. Elisei and L. Latterini, *Langmuir*, 2000, **16**, 10351; (*c*) L. Mohanambe and S. Vasudevan, *J. Phys. Chem. B*, 2005, **109**, 22523; (*d*) S. Gago, T. Costa, J. S. de Melo, I. S. Gonçalves and M. Pillinger, *J. Mater. Chem.*, 2008, **18**, 894; (*e*) J. Bauer, P. Behrens, M. Speckbacher and H. Langhals, *Adv. Funct. Mater.*, 2003, **13**, 241; (*f*) L. Mohanambe and S. Vasudevan, *J. Phys. Chem. B*, 2006, **110**, 14345; (*g*) D. P. Yan, J. Lu, M. Wei, J. Ma, D. G. Evans and X. Duan, *Phys. Chem. Chem. Phys.*, 2009, **11**, 9200; (*h*) D. P. Yan, J. Lu, J. Ma, M. Wei, D. G. Evans and X. Duan, *Phys. Chem. Chem. Phys.*, 2010, **12**, 15085; (*i*) D. P. Yan, J. Lu, M. Wei, S. H. Qin, L. Chen, S. T. Zhang, D. G. Evans and X. Duan, *Adv. Funct. Mater.*, 2011, **21**, 2497; (*j*) D. P. Yan, J. Lu, J. Ma, S. Qin, M. Wei, D. G. Evans and X. Duan, *Angew. Chem., Int. Ed.*, 2011, **50**, 7037; (*k*) E. Káfuňková, C. Taviot-Guého, P. Bezdicka, M. Klementová, P. Kovár, P. Kubát, J. Mosinger, M. Pospıšil and K. Lang, *Chem. Mater.*, 2010, **22**, 2481; (*l*) M. Jiřičková, J. Demel, P. Kubát, J. Hostomský, F. Kovanda and K. Lang, *J. Phys. Chem. C*, 2011, **115**, 21700; (*m*) D. P. Yan, J. Lu, J. Ma, M. Wei, S. Li, D. G. Evans and X. Duan, *J. Phys. Chem. C*, 2011, **115**, 7939; (*n*) D. P. Yan, J. Lu, M. Wei, D. G. Evans and X. Duan, *Phys. Chem. Chem. Phys.*, 2012, **14**, 8591.
13 (*a*) J. R. Heldt, J. Heldt, M. Józefowicz and J. Kamiński, *J. Fluoresc.*, 2001, **11**, 65; (*b*) J. D. Furman, A. Y. Warner, S. J. Teat, A. A. Mikhailovsky and A. K. Cheetham, *Chem. Mater.*, 2010, **22**, 2255; (*c*) Q. Yue, L. Yan, J.–Y. Zhang and E.-Q. Gao, *Inorg. Chem.*, 2010, **49**, 8647; (*d*) J. D. Furman, B. C. Melot, S. J. Teat, A. A. Mikhailovsky and A. K. Cheetham, *Phys. Chem. Chem. Phys.*, 2011, **13**, 7622; (*e*) D. P. Yan, R. Gao, M. Wei, S. D. Li, J. Lu, D. G. Evans and X. Duan, *J. Mater. Chem. C*, 2013, **1**, 997.
14 P. J. Sideris, U. G. Nielsen, Z. Gan and C. P. Grey, *Science*, 2008, **321**, 113.
15 (*a*) A. M. Aicken, I. S. Bell, P. V. Coveney and W. Jones, *Adv. Mater.*, 1997, **9**, 496; (*b*) S. P. Newman, S. J. Williams, P. V. Coveney and W. Jones, *J. Phys. Chem. B*, 1998, **102**, 6710; (*c*) S. P. Newman, T. D. Cristina, P. V. Coveney and W. Jones, *Langmuir*, 2002, **18**, 2933; (*d*) H. Li, J. Ma, D. G. Evans, T. Zhou, F. Li and X. Duan, *Chem. Mater.*, 2006, **18**, 4405; (*e*) M.-A. Thyveetil, P. V. Coveney, H. C. Greenwell and J. L. Suter, *J. Am. Chem. Soc.*, 2008, **130**, 4742.
16 (*a*) M. P. Allen and D. J. Tildesley, *Computer Simulation of Liquids*, Clarendon, Oxford, 1987; (*b*) A. R. Leach, *Molecular Modeling, Principles and Applications*, Pearson Education Ltd, England, 2nd edn 2001.
17 (*a*) B. Delley, *J. Chem. Phys.*, 1990, **92**, 508; (*b*) B. Delley, *J. Chem. Phys.*, 2000, **113**, 7756; (*c*) *Dmol3 Module, MS Modeling*, Version 2.2; Accelrys Inc.: San, Diego, CA, 2003; (*d*) J. R. Maple, M.-J. Hwang, T. P. Stockfisch, U. Dinur, M. Waldman, C. S. Ewig and A. T. Hagler, *J. Comput. Chem.*, 1994, **15**, 162; (*e*) D. P. Yan, J. Lu, M. Wei, H. Li, J. Ma, F. Li, D. G. Evans and X. Duan, *J. Phys. Chem. A*, 2008, **112**, 7671; (*f*) Y. Zhang, H. Tan, J. Zhao, X. Li, H. Ma, X. Chen and X. Yang, *Phys. Chem. Chem. Phys.*, 2012, **14**, 9067; (*g*) J. P. Perdew, J. A. Chevary, S. H. Vosko, K. A. Jackson, M. R. Pederson, D. J. Singh and C. Fiolhais, *Phys. Rev. B: Condens. Matter*, 1992, **46**, 6671.
18 M. Bellotto, B. Rebours, O. Clause, J. Lynch, D. Bazin and E. Elkaim, *J. Phys. Chem.*, 1996, **100**, 8527.
19 (*a*) A. T. Petkova, R. D. Leapman, Z. H. Guo, W. M. Yau, M. P. Mattson and R. Tycko, *Science*, 2005, **307**, 262; (*b*) J. K. Harper, J. C. Facelli, D. H. Barich, G. McGeorge, A. E. Mulgrew and D. M. Grant, *J. Am. Chem. Soc.*, 2002, **124**, 10589.
20 (*a*) H. Günzler and H. Gremlich, in *IR Spectroscopy: An Introduction*, Wiley-VCH, Verlag GmbH, 2002; (*b*) J. H. Lee, S. W. Rhee and D. Y. Jung, *Chem. Mater.*, 2004, **16**, 4774.
21 B. Valeur, *Molecular Fluorescence: Principles and Applications*, Wiley-VCH Verlag GmbH, 2001.
22 (*a*) D. P. Yan, S. H. Qin, L. Chen, J. Lu, J. Ma, M. Wei, D. G. Evans and X. Duan, *Chem. Commun.*, 2010, **46**, 8654; (*b*) D. P. Yan, J. Lu, J. Ma, M. Wei, D. G. Evans and X. Duan, *Angew. Chem., Int. Ed.*, 2011, **50**, 720.
23 (*a*) F. De Angelis, S. Fantacci, A. Selloni, M. K. Nazeeruddin and M. Grätzel, *J. Am. Chem. Soc.*, 2007, **129**, 14156; (*b*) M. Freitag and E. Galoppini, *Energy Environ. Sci.*, 2011, **4**, 2482.

